Science Platform and Attitude Subsystem In-Flight Calibration for the Galileo Spacecraft

Samad A. Hayati* and John Y. Lai†
Jet Propulsion Laboratory, California Institute of Technology, Pasadena, California

This paper presents a design methodology and the results of an in-flight calibration simulation study for a combined star scanner/gyro/scan platform for the dual-spin Galileo spacecraft. The design process involves three separate steps: the construction of an error model, the development of the calibration model, and the selection of the appropriate estimation technique. A major innovation is the development of these models, which are unique to the Galileo design. A unified procedure was developed to allow simultaneous calibration of the three subsystems. However, provisions were also made in the software to calibrate each subsystem separately whenever the necessary a priori information is available.

I. Introduction

THE dual-spin configured Galileo spacecraft, scheduled to be launched in 1986, will orbit Jupiter to conduct scientific investigations of the planet and its satellites. A probe, which will be released prior to Jupiter orbit insertion, is programmed to follow an impact trajectory for atmospheric investigations. For attitude determination (AD), the spacecraft is equipped with a star scanner that can detect stars and their locations with respect to the spacecraft body frame. In addition, two dual-axis gyros are employed for inertial AD whenever the star scanner is inoperative during certain phases of the mission (e.g., maneuvers). The gyros are also used to stabilize the science platform for inertial pointing of the various instruments mounted on it.

To satisfy the stringent requirements for attitude determination and control and the science platform pointing,[1] it is necessary to calibrate the attitude sensors as well as their mounting and structural misalignments. To assess these errors, both ground and in-flight calibrations are required. For in-flight calibration, the basic approach is to compare the celestial sensor data, which is obtained from the star scanner or platform-mounted imaging subsystem, with inertial sensor data from the gyros. Any discrepancy in these measurements is assumed to be caused by various subsystem error sources, which can be estimated. The error estimates are subsequently uplinked to the spacecraft for improved AD.

In Secs. II and III the spacecraft configuration and the sensors are described. In Sec. IV, modeling of the various error sources is defined. The calibration algorithm is described in Secs. V and VI and the simulation results are presented in Sec. VII. Section VIII provides a summary and conclusion.

II. Spacecraft Configuration

Figure 1 depicts the deployed Galileo spacecraft. It is comprised of three major parts: the spun section, the despun section, and the entry probe.

The spun section, or rotor, carries an unfurlable high-gain antenna, which is normally Earth pointed with an accuracy of 3.1 mrad (accuracy figures correspond to 99.73% probability), a V-slit star scanner, a retropropulsion module composed of a single 400 N engine, two clusters of 10 N thruster pods and fuel tanks, the radioisotope thermoelectric generators located on two booms, and the science boom that carries the fields and particles instruments. When operating in dual-spin configuration, the rotor spins at 3.15 rpm to induce a large angular momentum for attitude stabilization.

The despun section, or stator, carries the scan platform, the despun electronics, the probe, and the probe relay antenna. In the dual-spin mode, the stator provides pointing capability for the scan platform. Two actuators articulate the scan platform. The first, the clock actuator, rotates the stator about the rotor Z axis and the second, the cone actuator, slews the scan platform about the stator Y axis. The rotations are sensed by 16 bit optical encoders with 20 arcsec resolution.

III. Sensors

The rotor-mounted star scanner is employed as a celestial sensor for the Galileo spacecraft. It consists of a set of refractive optics that project the star field images onto V-slit reticles. One of the slits, called the clock slit, will provide the clock positions of the stars detected on the spacecraft body frame. The other, termed the cone slit, is slanted with respect to the former to provide the cone positions of the stars. To evaluate the star cone and clock position requires that spin rate information be available. In general, spin rate can be determined from the repetitive star pattern over several revolutions. However, an a priori spin rate estimate from a different sensor, e.g., sun sensor and gyro, is still required for initialization.

Accurate determination of the spacecraft inertial attitude is accomplished with a pair of position sensing two-axis gyros mounted directly on the scan platform. The two gyros and their pick-off preamps are housed in the gyro sensor subassembly (GSS). The input axes of the gyros are oriented to measure spacecraft motion in three orthogonal directions.

The imaging science requirements impose scan platform pointing accuracies of 3.4 mrad for a single frame and 0.125 mrad for frame-to-frame imaging. The SSI camera has an 800×800 element charge-coupled device (CCD) image sensor array (8×8 mrad field of view) composed of solid-state silicon detectors. The camera, in addition to obtaining high-resolution images of the Jovian system, is used for optical navigation.

IV. Error Sources and Modeling

The error sources are represented by small angle rotations about each of the axes of a nominal coordinate system listed

Presented as Paper 81-1810 at the AIAA Guidance and Control Conference, Albuquerque, N. Mex., Aug. 19-21, 1981; received Sept. 30, 1981; revision received Dec. 3, 1982.

*Member, Technical Saff, Koboties and Teleoperations Corp. Member AIAA.
†Member, Technical Staff, Guidance and Control Sections.

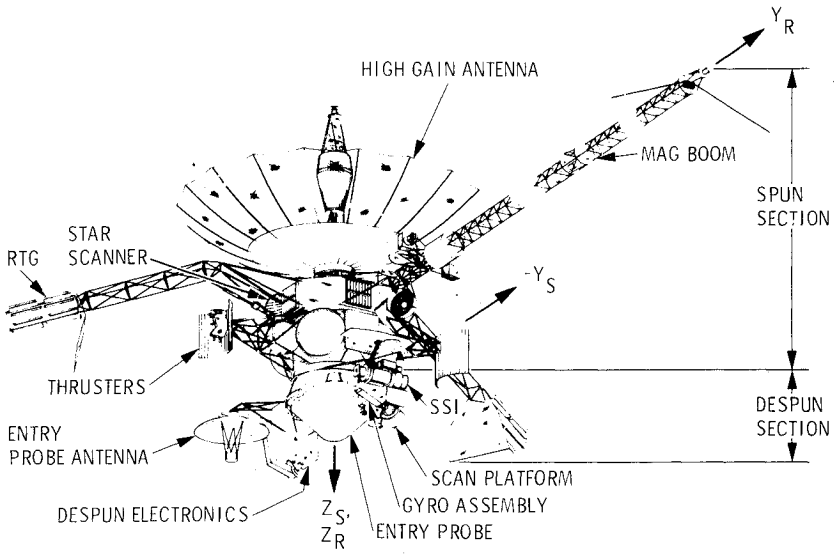

Fig. 1 Deployed Galileo spacecraft.

Table 1 Coordinate system definitions

1) Earth mean equator and equinox, epoch of 1950, E	An inertially fixed coordinate system (Ref. 2)
2) Stator coordinate system, S	Computed from the onboard estimate of the initial attitude; see Fig. 1.
3) Rotor coordinate system, R	Rot* $(-\theta_t, 3)$ from S θ_t = clock encoder reading
4) Star scanner bore sight coordinate system, B	Rot $(\chi,1)$ Rot $(\zeta,2)$ Rot $(\gamma,3)$ from R χ, ζ, and γ constant angles
5) Star scanner slit coordinate system, Li, $i=1,2$	$\chi=1$: Rot $(\Delta\gamma,3)$ from β $1\ i=2$: Rot $(\beta,1)$ from β
6) Cone gimbal coordinate system, C	Nominally identical to S
7) Scan platform coordinate, P	Rot $(\pi+\phi_t, 2)$ from C ϕ_t = cone encoder reading
8) Gyro system subassembly coordinate	Rot $(-\pi/2,3)$ Rot $(3\pi/4, 1)$ from P
9) Solid-state imaging camera coordinate system, I	Nominally identical to P
10) Line and pixel coordinate system, LP	See Fig. 2

[a] Rot (α,i) = rotation by an angle α about the ith axis. The order of rotation is from right to left.

in Table 1. When there exists an a priori estimate from either ground or previous in-flight calibration, the error vector can be divided into two parts

$$\mathbf{e} = e + \delta \tag{1}$$

Here, e represents the a priori estimate and δ is the variation about e to be estimated.

Most likely, the axis of rotation will not be one of the reference axes. The general direction cosine matrix relating two coordinate systems is given by

$$^2\Upsilon^1 = I\cos\psi + (1-\cos\psi)dd^T - (dx)\sin\psi \tag{2}$$

Coordinate system 2 is obtained by rotating coordinate system 1 at an angle ψ about a unit vector d.

The x operator for vector $d=(d_x,d_y,d_z)^T$ is defined by

$$dx \triangleq \begin{bmatrix} 0 & -d_z & d_y \\ d_z & 0 & -d_x \\ -d_y & d_x & 0 \end{bmatrix} \tag{3}$$

When ψ is small, the orthogonal transformation $^2\Upsilon^1$ is approximated by

$$^2\Upsilon^1 = I - (\psi d)x \tag{4}$$

Since vector additions apply to small-angle rotations, ψd can be represented by three rotations about the coordinate system axes; thus,

$$^2\Upsilon^1 = I - \mathbf{e}x \tag{5}$$

Three separate coordinate systems are defined for each subsystem: nominal, predicted, and true coordinate systems. A predicted coordinate system is obtained by e rotation of a nominal coordinate system. Similarly, a true coordinate system is arrived at by rotating the predicted coordinate system by δ. The following relations exist between these three coordinate systems:

$^2\mathrm{T}^1$ = nominal transformation from 1 to 2
$^2T^1 = (I-\mathbf{e}x)\,^2\mathbf{T}^1$ = predicted transformation from 1 to 2
$^2\Upsilon^1 = (I-\delta x)\,^2T^1$ = true transformation from 1 to 2

When there are several error rotations in a sequence of transformations, they all may be mapped to a desired coordinate system. If $\mathbf{e}_i$ is defined in the ith coordinate system, the true transformation relating the coordinate system 0 to coordinate system n is

$$^n\Upsilon^0 = \prod_{i=0}^{n-1} (I-\mathbf{e}_{n-i}x)^{n-i}\mathrm{T}^{n-i-1}$$

If $\mathbf{e}$ is the resultant of all the error vectors defined in the coordinate system n, we have

$$^n\Upsilon^0 = (I-\mathbf{e}x)\,^n\mathrm{T}^0 \tag{6}$$

where

$$^n\mathrm{T}^0 = \prod_{i=0}^{n-1} {}^{n-i}\mathrm{T}^{n-i-1}$$

and **e** is given by

$$\mathbf{e} = \mathbf{e}_n + \sum_{i=1}^{n-1} {}^{n}\mathrm{T}^{i}\mathbf{e}_i \tag{7}$$

Since the onboard AD requires only the orientations of the slit normal vectors in the rotor coordinate,[3] the scanner misalignment errors are lumped into two error rotations about the X and Z axes of each slit coordinate system. The true slit normal can then be expressed as

$$\mathbf{n}_i = (I + \mathbf{e}_{Li}x)\begin{bmatrix} 0 \\ 1 \\ 0 \end{bmatrix}, \quad i = \begin{cases} 1 \text{ clock slit} \\ \\ 2 \text{ cone cone} \end{cases} \tag{8}$$

where $\mathbf{e}_{Li}$ are the slit misalignment error vectors.

Misalignments for each gyro input axis are modeled by two small angle rotations about the two orthogonal axes perpendicular to its nominal orientation in the G coordinate system. The true rates in G are given by

$$\omega_G = \mathrm{E}\omega \tag{9}$$

where E is an error matrix defined by

$$\mathrm{E} = \begin{bmatrix} 1 & -\mathrm{e}_2 & -\mathrm{e}_1 \\ \mathrm{e}_4 & 1 & \mathrm{e}_3 \\ -\mathrm{e}_5 & \mathrm{e}_6 & -1 \end{bmatrix}$$

and ω is the body rate along the three-gyro input axes.

To account for the scale factor, drift, and random measurement error, the following gyro model is assumed:

$$\omega = (I + \mathrm{K})(\omega_M + \nu_G) + \mathbf{d} \tag{10}$$

where K is a diagonal scale factor matrix, ω_M the measured rate vector, ν_G the random measurement error vector, and **d** the gyro drift vector.

By expanding Eqs. (9) and (10) to the first order, ω_G can be written as

$$\omega_G = \Omega + D\delta_G + F\nu_G = \Omega + \omega_e \tag{11}$$

where

$$\Omega = E[(I+K)\omega_M + d], \quad F = E(I+K),$$

$$\delta_G = \begin{bmatrix} \delta_K \\ \delta_d \\ \delta_e \end{bmatrix}$$

and

$$D = \begin{bmatrix} \omega_{M1} & 0 & 0 & 1 & 0 & 0 & -\omega_{M3} & -\omega_{M2} & 0 & 0 & 0 & 0 \\ 0 & \omega_{M2} & 0 & 0 & 1 & 0 & 0 & 0 & \omega_{M3} & \omega_{M1} & 0 & 0 \\ 0 & 0 & -\omega_{M3} & 0 & 0 & -1 & 0 & 0 & 0 & 0 & -\omega_{M1} & \omega_{M2} \end{bmatrix}$$

In the above equations, K is the predicted scale factor matrix and δ_K the variational vector of the scale factors obtained by subtracting the diagonal elements of K and K,

$$\delta_d = \mathbf{d} - d, \ \delta_e = [\mathrm{e}_1 - e_1, \ldots, \mathrm{e}_6 - e_6]^T$$

To evaluate the predicted transformation ${}^{G}T^{G_0}$ from Ω, the differential equation

$$\frac{\mathrm{d}}{\mathrm{d}t}({}^{G}T^{G_0}) = -(\Omega x)\,{}^{G}T^{G_0} \tag{12}$$

Due to the presence of the unknown ω_e in Eq. (11), the true transformation ${}^{G}\mathrm{T}^{G_0}$ can be defined as

$${}^{G}\mathrm{T}^{G_0} = (I - \epsilon x)\,{}^{G}T^{G_0} \tag{13}$$

By differentiating Eq. (13), a differential equation can be obtained for the error vector ϵ as

$$\dot{\epsilon} = -(\Omega x)\epsilon + \omega_e \tag{14}$$

Note that the product term between ω_e and ϵ is assumed to be small and negligible. Equation (11) indicates that ω_e contains both systematic δ_G and random ν elements. Therefore, ϵ can be considered separately by virtue of superposition of a linear system. Let

$$\epsilon = \epsilon_S + \epsilon_R$$

then

$$\dot{\epsilon}_S = -(\Omega x)\epsilon_S + D\delta_G, \qquad \epsilon_S(0) = 0 \tag{15}$$

and

$$\dot{\epsilon}_R = -(\Omega x)\epsilon_R + F\nu_G, \qquad \epsilon_R(0) = 0 \tag{16}$$

δ_G can be assumed to be time invariant during the calibration period; therefore,

$$\epsilon = G\delta_G + \epsilon_R \tag{17}$$

where the partial matrix G is obtained by solving the matrix differential equation

$$\dot{G} = -(\Omega x)G + D, \qquad G(0) = 0$$

All the error sources affecting stator to scan platform transformations are modeled by rotational error vectors $\mathbf{e}_c$ about the nominal cone gimbal coordinate system (see Table 1 for definitions). A small angle rotation about the Z_C axis represents the clock encoder null offset plus the clock misalignment of the cone gimbal. The cone gimbal nonorthogonality with respect to the spacecraft Z axis (or the stator Z axis) is accounted for by an error rotation about the X_C axis.

The cone encoder error is modeled by a rotation about the scan platform Y axis. Due to hysteresis errors in the cone encoder readings, the error magnitude depends on the direction of the last slewing of the scan platform

$$\theta = \theta_M - \mathrm{e}_H \mathrm{sgn}(\Delta\theta) - \mathrm{e}_N \tag{18}$$

where θ is the true cone angle, θ_M the cone encoder reading, e_H the hysteresis error, e_N the cone encoder null offset, and $\Delta\theta$ the last cone angle change.

These error rotations are defined by $\mathbf{e}_C$ as

$$\mathbf{e}_C = (\mathrm{e}_{Cx}, -\mathrm{e}_N - \mathrm{e}_H \mathrm{sgn}(\Delta\theta), \mathrm{e}_{C_z})^T \tag{19}$$

and hence the transformation between the S and C frames is given by

$${}^{C}\mathrm{T}^{S} = (\mathrm{I} - \mathbf{e}_c x)\,{}^{C}\mathrm{T}^{S}$$

Three small angle rotations model the SSI camera boresight misalignments and are designated by $\mathbf{e}_I$. In addition to these misalignments, an error model for the optics must be con-

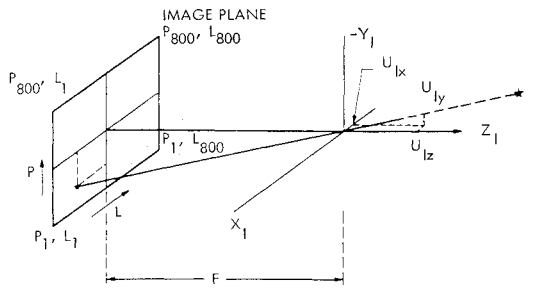

Fig. 2 Solid-state imaging camera schematic.

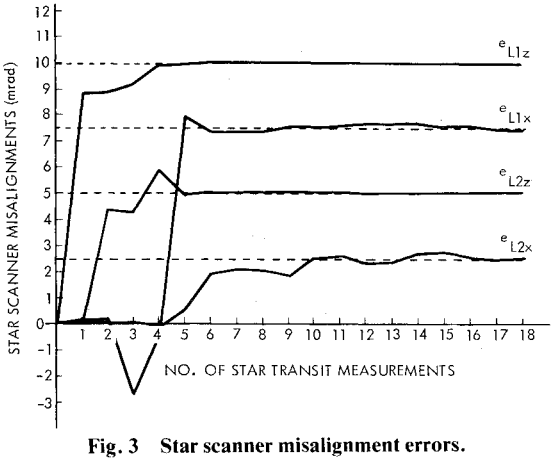

Fig. 3 Star scanner misalignment errors.

pressed in the I coordinate system to its image line and pixel coordinate (Fig. 2), is

$$\begin{bmatrix} L \\ P \end{bmatrix} = \begin{bmatrix} L_0 \\ P_0 \end{bmatrix} + \frac{kf}{u_{I_z}} \begin{bmatrix} u_{I_x} \\ u_{I_y} \end{bmatrix} \tag{20}$$

where (L_0, P_0) are the line and pixel coordinates of the center of the image plane, k the scale factor, and f the focal length. The errors associated with the camera optics are e_k and e_f.

To initialize the gyro attitude at time $t=0$, the onboard rotor attitude is utilized. The corresponding initialization error is denoted by $\mathbf{e}_A$ and hence

$$^{R_0}\Upsilon^{E} = (I - \mathbf{e}_A x)\,^{R_0}T^{E} \tag{21}$$

V. Calibration

In general, in-flight calibration is the process of estimating error parameters by using data received from the spacecraft. The calibration model is a set of observation equations that relate the error model parameters described in Sec. IV to the quantities measured by the actual system. Since, in general, the star crossing times for the star scanner do not coincide with the imaging times, two sets of observation equations are derived by considering two paths: the star scanner/gyro path and the SSI camera/gyro path.

To define an observation model for the star scanner/gyro path, the orthogonality condition of the star vector (**s**) and the slit normal vector $\mathbf{n}_i$ is utilized. To express these two vectors in the same coordinate system, a series of transformations are required to map $\mathbf{n}_i$ to the E frame using the gyro information as

$$\mathbf{s}^T \overset{E\,R_0}{\Upsilon} \overset{R_0\,S_0}{\Upsilon} \overset{S_0\,C_0}{\Upsilon} \overset{C_0\,P_0}{\Upsilon} \overset{P_0\,G_0}{\Upsilon} \overset{G_0\,G}{\Upsilon} \overset{G\,P}{\Upsilon} \overset{P\,C}{\Upsilon} \overset{C\,S}{\Upsilon} \overset{S\,R}{\Upsilon} \overset{R\,L_i}{\Upsilon} \mathbf{n}_i = 0 \tag{22}$$

Equation (22) may be written as

$$\mathbf{s}^T \overset{E\,L_i}{\Upsilon} \mathbf{n}_i = \mathbf{s}^T \overset{E\,L_i}{T} (I + \delta_i x) n_i = 0 \tag{23}$$

Using the error models developed in the previous section, the equivalent error vector (δ_i) can be obtained from Eq. (23) to the first order as

$$\delta_i = C_i \epsilon_B, \qquad i = 1,2 \tag{24}$$

where

$$C_1 = [\overset{L_1\,R_0}{T},\ \overset{L1\,C_0}{T}\ N_0 - \overset{L1\,C}{T}\ N_t,\ \overset{L1\,G}{T}\ G, U, 0_{3\times 3},\ \overset{L1\,G}{T}]$$

$$C_2 = [\overset{L2\,R_0}{T},\ \overset{L2\,C_0}{T}\ N_0 - \overset{L2\,C}{T}\ N_t,\ \overset{L2\,G}{T}\ G, 0_{3\times 3}, U,\ \overset{L2\,G}{T}]$$

$$U = \begin{bmatrix} 1 & 0 & 0 \\ 0 & 0 & 0 \\ 0 & 0 & 1 \end{bmatrix}$$

$$N_t = \begin{bmatrix} 1 & 0 & 0 & 0 \\ 0 & -\operatorname{sgn}[\Delta\theta(t)] & -1 & 0 \\ 0 & 0 & 0 & 1 \end{bmatrix}$$

$$\epsilon_B^T = [\delta_A^T, (\delta_{Cx}, \delta_H, \delta_N, \delta_{Cz}), \delta_G^T, \delta_{L1}^T, \delta_{L2}^T, \epsilon_R^T] = [\epsilon_D^T, \epsilon_R^T] \tag{25}$$

By expanding Eq. (23) and substituting from Eq. (24), an observation equation can be established.

$$\mathbf{s}^T \overset{E\,Li}{T}\, n_i = \mathbf{s}^T \overset{E\,Li}{T}\, (n_i x) C_i \epsilon_B \tag{26}$$

or

$$\mu_i = H_i \epsilon_B$$

The error vector ϵ_B consists of a total of 26 error sources, of which the first 23 errors (ϵ_D) can be assumed to be time invariant during the calibration period. In addition, there are other error sources, such as the star scanner transit time errors and the clock/cone encoder resolutions, which are random in nature. However, they can all be lumped together as a single-measurement noise (ν_B) with covariance R_B to give

$$\mu_i = H_i \epsilon_B + \nu_B \tag{27}$$

At each star transit, the scalar μ_i and the vector H_i can be evaluated from telemetry data for estimate updates.

With ϵ_D assumed to be time invariant, and using Eq. (16), the system equation can be defined as

$$\begin{bmatrix} \dot{\epsilon}_D \\ \dot{\epsilon}_R \end{bmatrix} = \begin{bmatrix} 0 & 0 \\ 0 & -\Omega x \end{bmatrix} \begin{bmatrix} \epsilon_D \\ \epsilon_R \end{bmatrix} + \begin{bmatrix} 0 \\ F \end{bmatrix} \nu_G$$

$$\dot{X} = A(t) X + B\nu_G \tag{28}$$

Since the observation equation is valid only at discrete time points (star transits), it is necessary to discretize the system equation in order that the Kalman estimator can be applied. So,

$$X(k+1) = \phi(k+1,k) X(k) + \Gamma(k+1) \tag{29}$$

where

$$\dot{\phi}(t,t_0) = A(t)\phi(t,t_0), \qquad \phi(t_0,t_0) = I \tag{30}$$

and

$$\Gamma(k+1) = \int_k^{k+1} \phi(k+1,\tau) B \nu_G \, d\tau \tag{31}$$

It can be shown

$$E\{\Gamma(k+1)\}=0$$

$$E\{\Gamma(k+1)\Gamma^T(k+1)\}=\int_k^{k+1}\phi(k+1,\tau)BQB^T\phi^T(k+1,\tau)\,d\tau$$

$$=V_\Gamma(k+1) \tag{32}$$

where

$$E\{\nu_G(\tau_1)\nu_G^T(\tau_2)\}=Q\delta(\tau_1-\tau_2)$$

To improve numerical efficiency, it is desirable to express the covariance marix $V_\Gamma(k+1)$ as a differential equation rather than as an integral equation. By differentiating Eq. (32), it can be shown that $V_\Gamma(k+1)$ can be obtained by solving the Riccati equation for S as

$$\dot{S}=AS+SA^T+BQB^T$$

Since A is time varying, $S(k+1)$ can be obtained by numerical integration from k to $(k+1)$ with $S(k)=0$ as the initial condition. Then $V_\Gamma(k+1)$ is equal to $S(k+1)$. Having defined the system noise covariance matrix, a standard Kalman estimator can be applied as

$$\hat{X}(k+1)=\phi(k+1,k)\hat{X}(k)+K(k+1)[\mu(k+1)$$
$$-H(k+1)\phi(k+1,k)\hat{X}(k)]$$

$$P_p(k+1)=\phi(k+1,k)P_F(k)\phi^T(k+1,k)+V_\Gamma(k+1)$$

$$K(k+1)=P_p(k+1)H^T(k+1)[H(k+1)P_p(k+1)$$
$$\times H^T(k+1)+R(k+1)]^{-1}$$

$$P_F(k+1)=[I-K(k+1)H(k+1)]P_p(k+1)$$

for error parameter estimation.

The observables for the SSI camera/gyro path are obtained by comparing the coordinates of the measured star images to the computed (or predicted) star image locations. The latter are determined by reconstructing the spacecraft (or camera) attitude by propagating the telemetered initial spacecraft attitude through gyro information. The observation equation is derived by mapping the known star vector onto the camera image plane. This is done by incorporating the error rotational matrices in the relevant transformations and considering the fact that the measured star coordinates differ from the true image locations only by the measurement noise.

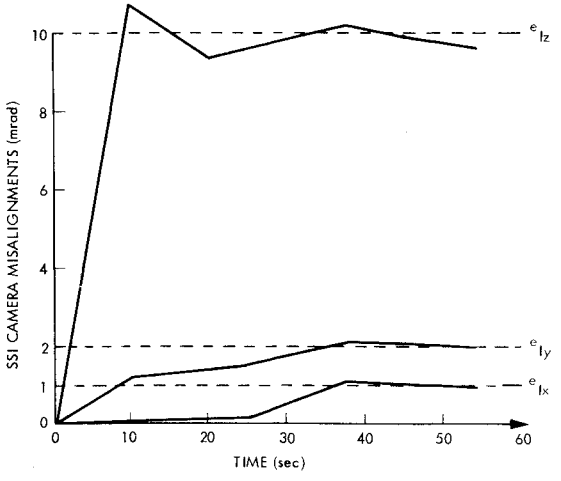

Fig. 4 Solid-state imaging camera errors.

A unit vector u_E, defined in E, of a star can be represented in the true I coordinate system by

$$\mathbf{u}_I=\overset{IE}{T}u_E \tag{33}$$

When all the error vectors are mapped onto the SSI coordinate system, Eq. (33) reduces to

$$\mathbf{u}_I=(I-\delta x)\overset{IE}{T}u_E \tag{34}$$

where δ is the net generalized error vector. The predicted star vector is computed from

$$u_I=\overset{IE}{T}u_E \tag{35}$$

and thus

$$\mathbf{u}_I-u_I=(u_Ix)\delta \tag{36}$$

The true transformation for the SSI camera is written as [see Eq. (20)]

$$\mathbf{a}=\begin{bmatrix}\mathrm{L}\\ \mathrm{P}\end{bmatrix}=\begin{bmatrix}L_0\\ P_0\end{bmatrix}+\frac{\mathrm{kf}}{\mathrm{u}_{Iz}}\begin{bmatrix}\mathrm{u}_{Ix}\\ \mathrm{u}_{Iy}\end{bmatrix} \tag{37}$$

where

$$\mathrm{k}=k+\delta_k,\qquad \mathrm{f}=f+\delta_f \tag{38}$$

The above notations are consistent with those defined for the error vectors. If a_M is defined as the vector of measured line and pixel for the image of a star, a_M and $\mathbf{a}$ differ only by the measurement noise which is the result of image resolution (10 μrad) and some possible unmodeled error sources. Thus we have

$$a_M=\mathbf{a}+\nu_I \tag{39}$$

The measurement noise ν_I is assumed to be zero mean Gaussian white noise process with the covariance matrix R_I.

The observable for this path is defined by a two-vector α as the difference between a_M and predicted line and pixel vector a,

$$\alpha=a_M-a \tag{40}$$

By linearizing Eq. (37) about a, the observable α is related to the error parameters of the optics

$$\mathbf{a}=a+\frac{\partial a}{\partial(f,k)}\begin{bmatrix}\delta_f\\ \delta_k\end{bmatrix}+\frac{\partial a}{\partial u_I}(\mathbf{u}_I-u_I) \tag{41}$$

Now the observable can be related to the error parameters by using Eqs. (36), (37), and (39-41) as

$$\alpha=L\epsilon_I+\nu_I \tag{42}$$

where L is the observation matrix defined by

$$L=\left\{\frac{\partial a}{\partial u_I}(u_Ix)\left[\overset{IR_0}{T},\ \overset{IC_0}{T}N_0,\ \overset{IG}{T}G,I_{3\times3}\right],\right.$$
$$\left.\frac{\partial a}{\partial(f,k)},\frac{\partial a}{\partial u_I}(u_Ix)\overset{IG}{T}\right\} \tag{43}$$

and ϵ_I is the error vector defined by

$$\epsilon_I^T=[\delta_A^T,(\delta_{Cx},\delta_H,\delta_N,\delta_{Cz}),\delta_G^T,\delta_I^T,(\delta_f,\delta_k),\epsilon_K^T]$$

There are 27 error parameters to be estimated in this path. The first 24 are considered to be constant parameters during each in-flight calibration. Denoting these by ϵ_F, we have

$$\epsilon_I = [\epsilon_F^T, \epsilon_R^T] \tag{44}$$

Equations (42-44) provide the observation model for the SSI camera/gyro path.

The estimator model for this path is similar to the one used for the star scanner/gyro path. Equations (28-32) can be used to define the state equations except that ϵ_D should be replaced with ϵ_F. Here a special form of discrete Kalman filter is employed to solve for the error parameters of Eq. (42). First, the a priori covariance matrix is propagated using

$$P_p(k+1) = \phi(k+1,k) P_F(k) \phi^T(k+1,k) + V_\Gamma(k)$$

Then, the new estimates together with their covariance matrix are obtained by solving the following equations:

$$\hat{\epsilon}_I(k+1) = P(k+1)\left[\sum_{i=1}^{m} L^T(k+1,i) R_I^{-1} \alpha(k+1,i) + P_p^{-1}(k+1)\epsilon_I(k)\right]$$

$$P(k+1) = \left[P_p^{-1}(k+1) + \sum_{i=1}^{m} L^T(k+1,i) R_I^{-1} L(k+1,i)\right]^{-1}$$

where

m = number of star images in the picture taken at time
$L(k+1,i)$ = partial matrix computed at time t_{k+1} for the ith star image
$P_p(k+1)$ = propagated a priori covariance matrix
$P(k+1)$ = updated covariance matrix
$\hat{\epsilon}_I(k+1)$ = a new estimate for the error parameters

VI. Combined Calibration

The error vectors ϵ_B and ϵ_I, as estimated by the star scanner/gyro path and the scan platform/gyro path, respectively, contain common error parameters. For a combined calibration, results obtained from either path will serve as a priori information for initialization of the other. A common data base is defined which includes a combined error vector (31×1)

$$\epsilon_C^T = [\delta_A^T, (\delta_{Cx}, \delta_H, \delta_N, \delta_{Cz}), \delta_G^T, \delta_{L1}^T, \delta_{L2}^T, \delta_f^T, (\delta_f, \delta_k), \epsilon_R^T]$$

and their covariance matrix P_C (31×31). To initialize either path, a selector matrix U is defined for retrieving the appropriate information from ϵ_C and P_C corresponding to the errors to be estimated. The selector matrix U is defined as

$$U = [q_1(i), q_2(j), \ldots, q_m(k)]^T$$

where $q^T(i)$ is the 31 row vector of zeros with a 1 at the ith location corresponding to the position of the error parameters to be estimated in $\epsilon_C \cdot m$ is the total number of errors to be estimated. Subsequently, the a priori information for initializing the path X can be obtained as

$$\epsilon_X = U_x \epsilon_C, \qquad P_X = U_x P_C U_x^T$$

When estimation is completed, the current estimates, ϵ_X, and covariance, P_X, are merged with the old data to obtain the updated combined data base as

$$P_C^* = \{P_C^{-1} + U_X^T [P_X^{-1} - (U_X P_C U_X^T)^{-1}] U_X\}^{-1}$$

$$\epsilon^* = P_C^* U_X P_X^{-1} [\epsilon_X - U_X \epsilon_C] + \epsilon_C$$

Table 2 Gyro calibration results

Error sources	Maximum residual errors: Star scanner/gyro path	Maximum residual errors: SSI camera/gyro path
Scale factors		
k_1	0.7×10^{-5}	0.4×10^{-5}
k_2	0.4×10^{-5}	1×10^{-5}
k_3	4×10^{-5}	2×10^{-5}
Drift rates, μrad/s		
d_1	0.2	0.47
d_2	1	1
d_3	0.2	1
Misalignments, mrad		
e_1	0.02	0.009
e_2	0.07	0.155
e_3	0.06	0.16
e_4	0.034	0.133
e_5	0.05	0.02
e_6	0.09	0.10

VII. Simulation

To validate the in-flight calibration algorithm and evaluate its performance, a simulation study was implemented. The spacecraft was modeled as a three-body system (rotor, stator, and scan platform). In most of these cases, the clock and cone slew rates are set to 3 and 5 deg/s, respectively, and data are collected for 60 s. These rates were set higher than the actual spacecraft maximum rates (1 deg/s) in order to reduce computation time. The data are then processed by the calibration program to estimate some or all of the subsystem error sources. The results of various test cases for each subsystem are briefly outlined below.

To calibrate the star scanner misalignments, transit times were generated for three reference stars. The scanner misalignment errors are in the range of 2.5-10 mrad. Random measurement noise is assumed to have 0.01 mrad (1σ). Figure 3 shows the results of this calibration. It can be observed that a maximum residual error of less than 0.08 mrad can be achieved after the 18 star transit data.

For the SSI camera/gyro path, the SSI camera is used as the celestial sensor where gyros serve as the inertial sensors. A total of 10 pictures of stars at various camera attitudes are processed to estimate the error parameters.

Even though only one star image per picture would be sufficient for calibration, up to six star images are used to improve the estimation accuracy. Figure 4 shows the result of estimation when only the SSI camera misalignments are considered. The image locations (line and pixel) are very sensitive to the x and y components of the boresight misalignment. Subsequently, they can be estimated to the image plane resolution accuracy (10 μrad). A small twist about the boresight, on the other hand, does not cause a large shift in the image coordinates. The residual error for twist is less than 1 mrad.

Either path can be utilized to estimate the gyro misalignments, drift rate, and scale factor errors. Table 2 shows the calibration residuals using either path.

Some error sources cannot be independently estimated using only one of the calibration paths. For example, the cone encoder null offset cannot be separated from the y component of the SSI camera misalignment. This error source is best estimated using the star scanner/gyro path. Conversely, the z component of the attitude initialization error cannot be separated from the clock components of the star scanner slit misalignments. This error source is best estimated using the SSI camera/gyro path. Thus by utilizing both paths, complete estimation of error sources can be realized.

VIII. Summary and Conclusion

A combined in-flight calibration algorithm for the Galileo star scanner, gyros, and solid-state imaging camera was developed. Two separate paths were defined, i.e., the star scanner/gyro path and the SSI camera/gyro path. A linear observation model was established for each path by com-

paring the celestial sensor data, star scanner, or SSI to the inertial sensor data and gyros. Any discrepancies were considered to be due to the various error sources and were subsequently estimated by a Kalman estimator. The results obtained from either path are then employed to initialize the processing of the other. Simulation programs were developed for algorithm validation and performance evaluation.

The numerical results obtained through computer simulations confirm the feasibility of the in-flight calibration algorithm.

Acknowledgments

The authors wish to acknowledge W.G. Breckenridge for his contributions to the development of the calibration model.

The research described in this paper was carried out by the Jet Propulsion Laboratory, California Institute of Technology, under contract with the National Aeronautics and Space Administration.

References

[1]Hayati, S.A. and Jahanshahi, M.H., "Galileo Spacecraft Pointing Accuracy Analysis," AIAA Paper 82-1459, Aug. 1982.

[2]Wertz, J.R., *Spacecraft Attitude Determination and Control,* D. Reidel Publishing Co., Boston, 1978.

[3]Wong, E.C. and Lai, J.Y., "Celestial Referenced Attitude Determination of Galileo Spacecraft," *Journal of Guidance, Control, and Dynamics,* Vol. 5, May-June 1982, pp. 307-312.